Journal of Alloys and Compounds 506 (2010) 172–178

Contents lists available at ScienceDirect

Journal of Alloys and Compounds

journal homepage: www.elsevier.com/locate/jallcom

High-strength and high-conductive Cu/Ag multilayer produced by ARB

L. Ghalandari*, M.M. Moshksar

Department of Materials Science and Engineering, School of Engineering, Shiraz University, Shiraz, Iran

ARTICLE INFO

Article history:
Received 2 February 2010
Received in revised form 24 June 2010
Accepted 30 June 2010
Available online 7 July 2010

Keywords:
ARB
Cu–Ag
Multilayer
Conductivity
TEM
SEM
Grain refinement

ABSTRACT

In this research high-strength and high-conductive multilayered Cu/Ag composites were produced by accumulative roll bonding (ARB) process for the first time using Cu and Ag strips up to nine cycles. Electrical resistivity changes were measured by the four-point-probe method and tensile tests were performed to investigate the mechanical behavior of ARB products. Finally scanning and transmission electron microscopy (SEM and TEM) were used to study the microstructure of the layers.

© 2010 Elsevier B.V. All rights reserved.

1. Introduction

Cu/Ag microcomposites have attracted interest because of their advantageous combination of excellent mechanical strength and relatively high electrical conductivity [1]. The microcomposites, have technological importance in windings in high-field magnet design electronic devices [2], advanced lead frames in large-scale integrated circuits [3], high magnetic field research, electric railways, heat transfer components, plasma-facing components [4], contacts and interconnect layers in semiconductor industry [5] and applications that require functional properties in the form of a non-equilibrium system [6].

To date, various methods including cold drawing combined with intermediate heat treatments (thermomechanical processing) for Cu/Ag wires [7,8] roll-bonding and subsequent diffusion annealing of Cu and Ag strips [9] thin film deposition [10,11], non-equilibrium processes including rapid quenching, plasma processes [12,13] and severe plastic deformation methods like mechanical alloying [14,15] have been developed for the fabrication of Cu–Ag microcomposites.

Thin film deposition with complicated processing has limited the potential applications for commercial use. Conventional thermomechanical processing methods are not suitable for manufacturing ultrafine grained (UFG) materials, since the minimum grain sizes that can be achieved are of the order of a few microns. Severe plastic deformation (SPD), which is a production method that consists of applying very large strains, often to a bulk sample, has proven to be a very effective way of fabricating UFG materials. UFG bulk metals and composites are considered very attractive structural materials since they are significantly stronger than their coarse-grained counterparts and retain good ductility. Additionally, UFG metals have improved corrosion resistance and potential for superplasticity at high strain rates and low temperatures [16,17]. Nevertheless, there has been few works on the production of Cu–Ag microcomposites with UFG microstructure by SPD. Recently Koa et al. [18] have used a combination of equal channel angular pressing and subsequent cold rolling to investigate the mechanical and electrical responses of nanostructured Cu–Ag alloy as a function of the imposed strain. By combining forced mixing and decomposition in ball-milled Cu50Ag50 powders, Zghal et al. [15] reported the formation of Cu/Ag nanocomposite with a very high hardness. Accumulative roll bonding (ARB) is one of the severe plastic deformation (SPD) processes which can produce bulk ultrafine grained (UFG) metallic materials [19,20]. Thus far, the ARB process has been applied to fabricate various ultrafine grained metallic sheets and multilayered composites owing to the relatively simple processing [21–24]. Ohsaki et al. [25] operated the ARB process on Cu–Ag eutectic alloy as attempts of bulk mechanical alloying.

In this study, the ARB process was used to produce Cu/Ag multilayered nanocomposites for the first time by choosing Cu and Ag strips as sandwich sheet layers. By this method we produced the microcomposite directly without any further processing. The gradual change of the microstructures as well as electrical and

* Corresponding author.
E-mail address: Ghalandari@shirazu.ac.ir (L. Ghalandari).

0925-8388/$ – see front matter © 2010 Elsevier B.V. All rights reserved.
doi:10.1016/j.jallcom.2010.06.172

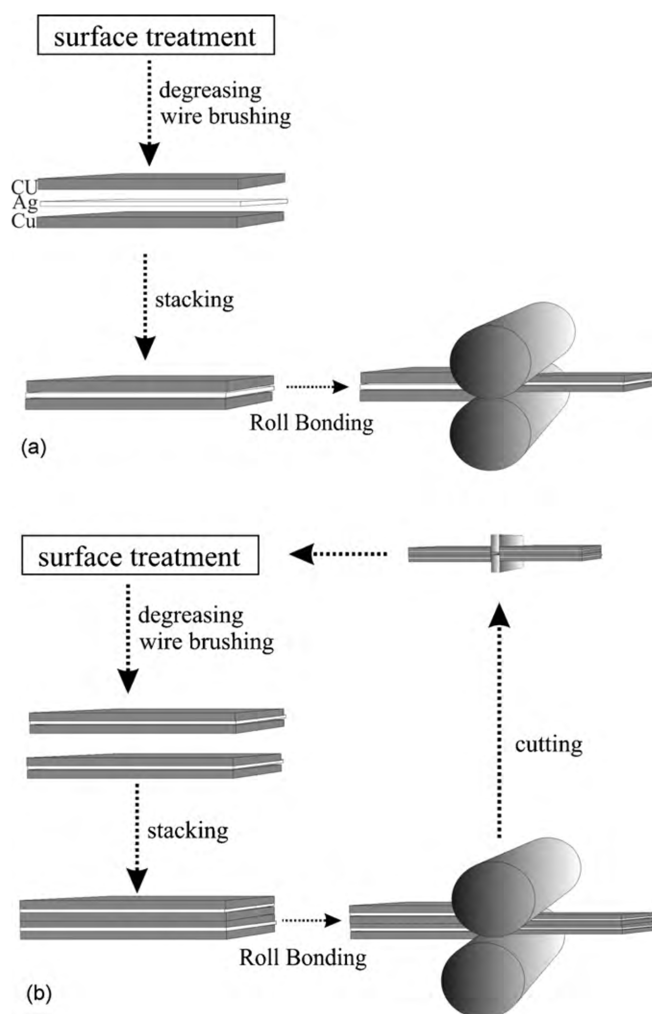

Fig. 1. Schematic illustration showing the principle of the accumulative roll bonding (ARB) process: (a) sandwich preparation cycle and (b) ARB cycles.

mechanical properties of the nanocomposite products were examined and discussed.

2. Experimental procedures

Commercially available copper of 1.0 mm thickness and pure silver of 0.1 and 0.2 mm thicknesses were cut into 3 mm × 150 mm. After degreasing and wire-brushing of the sheet surfaces, they were stacked in the manner of two copper layers with one core silver layer. The stacked sheets were first roll-bonded with 57% reduction in thickness, corresponding to the Von Mises equivalent strain of 0.99 (Fig. 1(a)).

Data regarding the sandwich preparation cycle including the entry thickness, the exit thickness, the reduction per cycle and the qualitative observations concerning the bonds are given in Table 1. These data showed that in the zero cycle, the bonds were generally well-formed as long as the reduction in the strip thickness was above a certain limit. This reduction was estimated to be approximately 56%. When the reduction was below this level, the bonding appeared weak. Therefore, the obtained roll-bonded sheets had two sandwich structure groups: Group1-Ag100 with a 100 μm thick Ag sheet in the core, Group2-Ag200 with a 200 μm thick Ag core.

Table 1
Examination of the sandwich preparation cycle.

Samples' number	$h_{in\ (mm)}$	$h_{out\ (mm)}$	Reduction %	Bonding quality
1	2.1	0.92	56	High
2	2.1	0.8	62	High
3	2.1	0.91	57	High
4	2.1	1.1	48	Low
5	2.1	1.4	33	Low

Examination results for the sandwich preparation cycle.

In the next stage, the roll-bonded sandwich was cut into two halves. The contacting surfaces of the halves were degreased, scratch-brushed and after being stacked over each other, roll-bonded with a fixed percentage of 50% reduction (the Von Mises equivalent strain of 0.8). This step, Fig. 1(b) of the process, was repeated up to nine cycles. After each cycle, the strips were prepared to be stacked and roll-bonded again. Therefore, 10 roll-bonding cycles were performed in total; one cycle in the first stage (denoted by zeroth cycle) and nine cycles in the second stage by the ARB process.

The roll-bonding experiments were carried out at room temperature without any lubricant using a laboratory rolling mill with a loading capacity of 20 ton. The roll diameter was 170 mm, and the rolling speed (ω) was 12 rpm. The tensile test samples with the tensile axes parallel to the rolling direction were 8 and 3 mm in gage length and width, respectively, which correspond to one-fifth of the JIS-5 standard dimensions [21]. These samples were machined from the products of the different cycles of the ARB process. Tensile tests were conducted at 25 °C and the initial strain rate of 10^{-4} s (using an Instron machine). The microstructures of Cu/Ag composites were studied using a scanning electron microscope (Vega©Tescan) in the back scattering mode before which the cross-section of the samples were ground, polished, etched in a solution of 100 ml C_2H_5OH, 5 ml HCl and 2 g $FeCl_3$ and repolished. The cross-sections of the samples were also examined using a transmission electron microscopy (200 kV, JEM-2100 LaB6). For this purpose, a thin slice from ND–RD plane was cut out from the rolled samples. The thickness of the sample was reduced to 50 μm by using sand paper followed by a dimple grinder. The thin slice was carefully glued to a copper grid and subjected to 12 h of precision ion milling with a radiation angle of 5°.

The X-ray diffraction patterns were recorded on the RD and TD plane surfaces of the ARB-processed sheets. 40 kV 30 mA Philip X'pert pro with negligible instrumental broadening using Cu Kα_1 radiation (λ = 0.15406 nm) in the range 2θ = 20–100° using a step size of 0.02° and a counting time of 0.4 s per step. The classic Williamson–Hall method [26] was used for measuring the crystallite size.

Electrical resistivity was measured at ambient temperature via the four-point-probe direct current technique from the surface of the samples. The resistivity of each sample was measured ten times and the mean value was reported.

3. Results and discussion

3.1. Critical reductions

In this investigation the amount of critical reduction to achieve sufficient copper-to-silver bonding strength in the zeroth cycle was (56%). Yang et al. [27] have recently investigated the bond strength of various metal multilayers produced by cold rolling of metal foils with different thermal conductivity. Results have indicated that the

Table 2
Variation in the thickness and number of layers by increasing ARB cycles.

ARB cycle (n)	Number of Cu layer (2×2^n)	Number of Ag layer (2^n)	Total layer number (3×2^n)	Equivalent strain (ε) ($0.98 + 0.8n$)	Final thickness of Cu (μm)	Final thickness of Ag (μm)
0	2	1	3	0.98	430	42.8
1	4	2	6	1.78	215	12.46265
2	8	4	12	2.58	107.5	7.15791
3	16	8	24	3.38	53.75	4.11114
4	32	16	48	4.18	26.875	2.36123
5	64	32	96	4.98	13.4375	1.35617
6	128	64	192	5.78	6.71875	0.77892
7	256	128	384	6.58	3.35938	0.44737
8	512	256	768	7.38	1.67969	0.25695
9	1024	512	1536	8.18	0.83984	0.14758

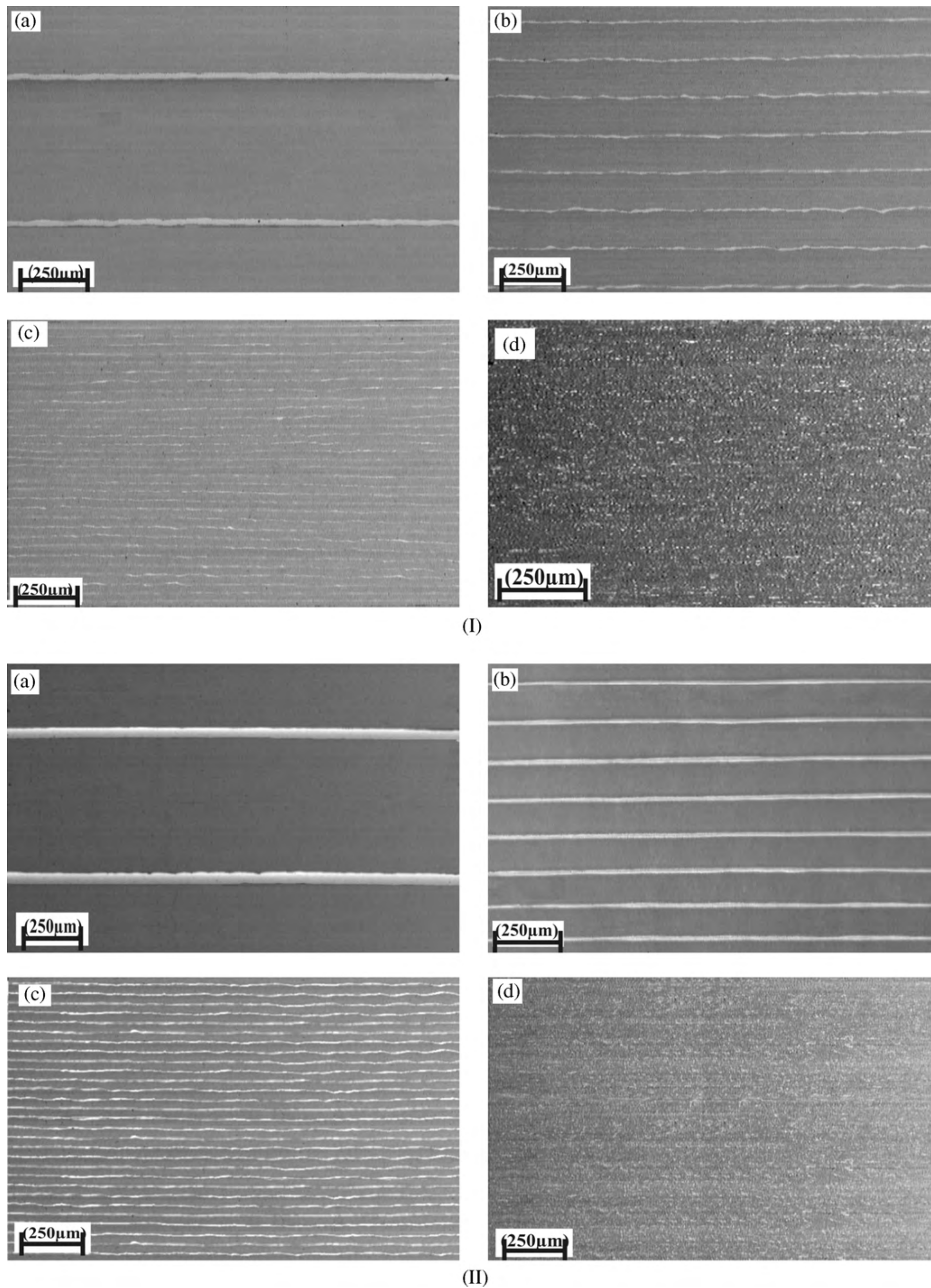

Fig. 2. SEM images of ARB-processed sheets in different cycles for (I) Ag100 and (II) Ag200 group samples: (a) first, (b) third, (c) fifth, (d) ninth cycle, the bright areas are silver.

metallic multilayer system with low thermal conductivity, exhibited relative high bond strength, while high thermal conductivity metal system may fail to be roll-bonded together. The thermal conductivity of silver is higher than that of copper. Therefore, to achieve a high Cu–Ag bonding quality, the critical reduction level in the zeroth cycle should be increased, whereas the conventional 50% reduction in the ARB cycles was sufficient since copper-to-copper bonding was required.

The SEM microstructures of the cross-sections of the composites, parallel to the rolling direction (the RD–ND plane), have been demonstrated in Fig. 2. It was shown that by increasing the ARB cycles, the thickness of the layers decreased and the number of layers increased in the same thickness. As verified in Table 2, there are 1536 layers, in the ninth cycle. The thickness of Cu and Ag layers in this cycle, are about 840 and 147 nm, respectively.

Fig. 3 shows the SEM micrographs of the ninth cycle of Ag100 and Ag200 sample groups. Due to the higher volume fraction of silver in Ag200 groups, a higher amount of bright area (Ag) is seen in Fig. 3c in comparison with Fig. 3a. The continuity of the constituent layers remained intact until the end of the ninth cycle. This was caused by the low hardness ratio of Cu and Ag as well as the high thickness ratio of the harder phase [28]. In addition, the elongated layer structure with multiple necking is depicted. As shown in this figure, in the ninth cycle of ARB process, the layer arrangement is irregular. This layer structure is a reflection of the inhomogeneous stress distribution in the multilayer. The main reason of stress inho-

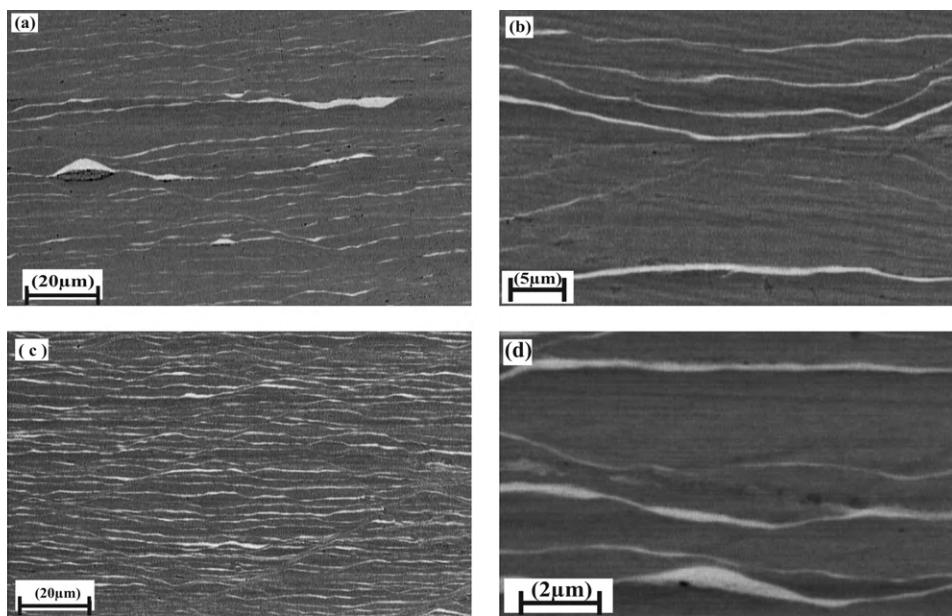

Fig. 3. SEM images of ninth cycle samples: (a and b) is for Ag 100 and (c and d) is for Ag200, the bright areas are silver.

mogeneities is due to two sources of friction, resulting from the rolls-sample contact surfaces and the interfaces of the multilayers themselves. This leads to a near-surface stress, as well as the residual stresses that occur within the layer boundaries due to the differences in the flow stresses between the component layers.

In Fig. 3a the amount of bright prominences is higher than that of Fig. 3c. This is a result of normal and frictional shear stresses between the layers. These stresses have a greater effect on the thinner silver layer in Ag100 group.

Classic Williamson–Hall method was used for evaluating the crystallite (dislocation cell or subgrain) size from XRD pattern for Cu layer in Ag200 group. The measurement results are shown in Fig. 4.

The mean crystallite size has been reduced to 40 nm after five cycles. The X-ray refers to the average measurements for the bulk volume. Local variations and spatial distribution of the nanograins cannot be traced. TEM observations provide the direct information on the spatial distribution.

Fig. 5 shows the TEM micrograph of the Ag200 in the fifth cycle of ARB. As can be seen, the grain size of the sample reached 102 nm in one direction (the ND direction) and 254 nm in rolling direction (the RD direction). Thus, an ultrafine grained microstructure was obtained. Surely in the higher ARB cycles smaller grains could be developed. It can be concluded that the average grain size measured by TEM is larger than that of the crystallite size calculated by XRD.

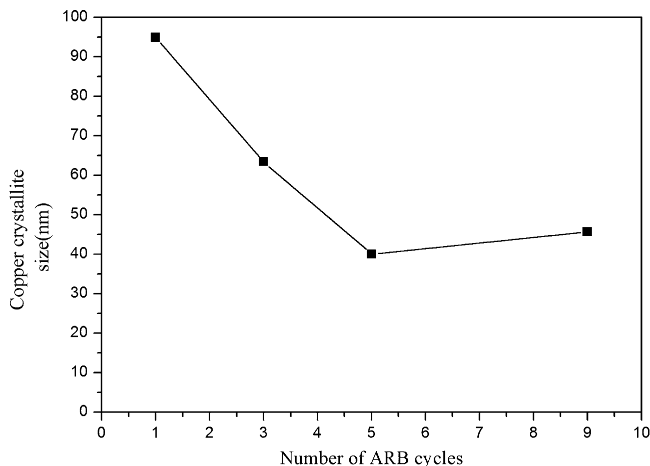

Fig. 4. The variations of copper layer crystallite size of the produced nanocomposites at various ARB cycles.

3.2. Mechanical properties of ARB specimens

3.2.1. The stress–strain curves

Fig. 6 shows the nominal stress–strain curves of the Cu–Ag sandwich sheets ARB-processed by various cycles. The shapes of the stress–strain curves in different ARB cycles follow a similar trend; however, they are completely different from the primary materials.

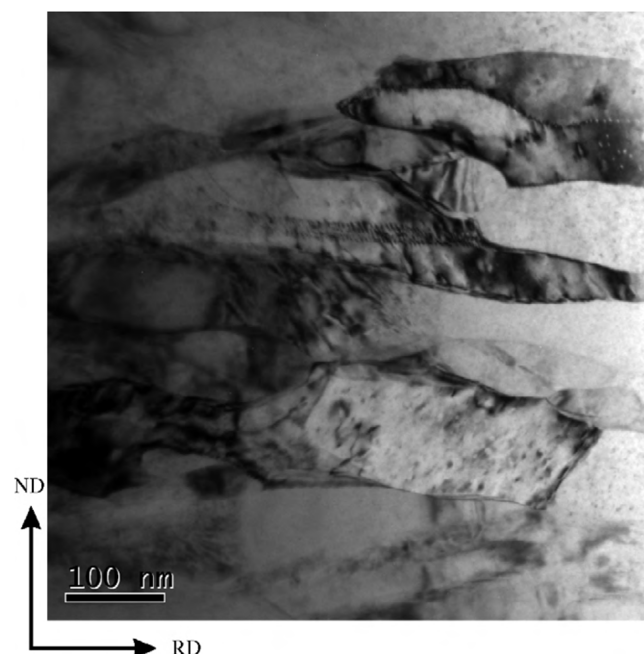

Fig. 5. TEM images of the fifth cycle of ARB for Ag200 samples group.

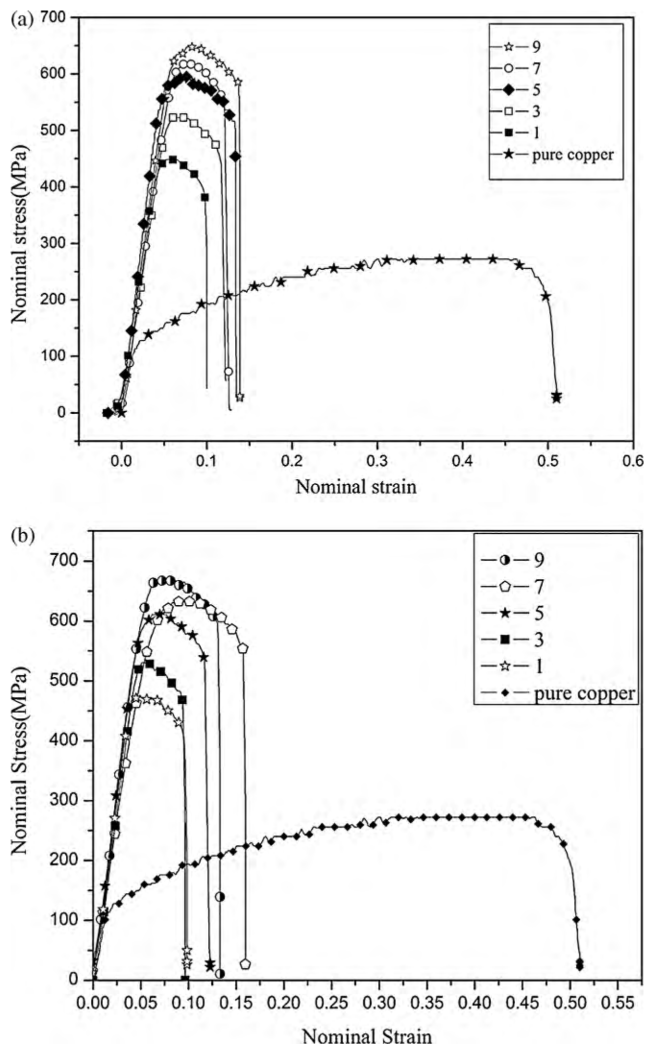

Fig. 6. Nominal stress–strain curves of the Cu–Ag sandwich sheets ARB-processed by various cycles of (a) Ag100 and (b) Ag200 samples.

The stress–strain curves of the ARBed samples show peak stress at the early stages of the tensile test. This indicates limited uniform elongation. The limited uniform elongation in the ultrafine grained materials could be a result of plastic instability conditions. The plastic instability condition is generally expressed by the following simple equation:

$$\frac{d\overline{\sigma}}{d\overline{\varepsilon}} \leq \overline{\sigma} \tag{1}$$

$\overline{\sigma}$ and $\overline{\varepsilon}$ are equivalent true stress and true strain, respectively. Grain refinement greatly increases the strength of the materials (the right-hand term in Eq. (1)). In addition, it has recently been shown that the work-hardening rate $d\overline{\sigma}/d\overline{\varepsilon}$ is not increased by grain refinement. The inability of ultrafine grained metals to accumulate dislocations owing to their small grain sizes, to absorb dislocations into the grain boundaries, and to saturate dislocations, can be responsible for the low strain hardening rate observed in the ultrafine grained metals [29]. As a result, in the ultrafine grained materials the plastic instability in tensile deformation occurs at the early stages of the tensile test, resulting in a limited uniform elongation under a few percent [30]. This phenomenon might cause the specimen to terminate in the fracture; however, concerning thin sheets, the diffuse necking is often followed by the second instability process, namely localized necking. These two types of necking are shown in Fig. 7 schematically. The onset of diffuse necking

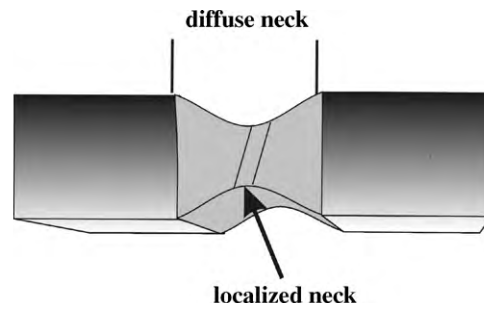

Fig. 7. Different types of necking.

occurs as a decrease in the width of the specimen. The appearance of the latter upcoming localized neck results in a slight decrease in the width of the specimen but the thickness along the necking band shrinks rapidly and soon thereafter the fracture occurs. Hill's localization theory indicates that localization can occur when:

$$\frac{d\overline{\sigma}}{d\overline{\varepsilon}} \leq \frac{\overline{\sigma}}{2} \tag{2}$$

The secondary strain localization depends on the shape factor of the tensile specimen (the width/thickness ratio) and the material strain hardening. A decrease the strain hardening parameter delays onset of localization [31].

As mentioned above, one of the distinguishing features of ultrafine grained metallic materials during tensile deformation, compared to coarse-grained ones, is that a considerably small amount of strain hardening occurs until fracture. Fig. 8 shows the variations in the localization delay during the ARB cycles. The localization delay was obtained by calculating the difference between the strain at the starting point of the diffuse neck and the secondary strain localization. As can be seen, in the early ARB cycles, localization occurs very soon as a result of the delamination of the bonded layers. As the number of layers increases, fewer instances of delamination are seen, leading to the delay of localization in the latter cycles.

3.2.2. Tensile strength

The strength (0.2% proof stress and tensile strength) and elongation (uniform elongation and total elongation) obtained from the curves are summarized in Fig. 9 as a function of the number of ARB cycles. It can be seen that the proof stress and tensile strength increases by increasing the strain up to nine ARB cycles. The tensile

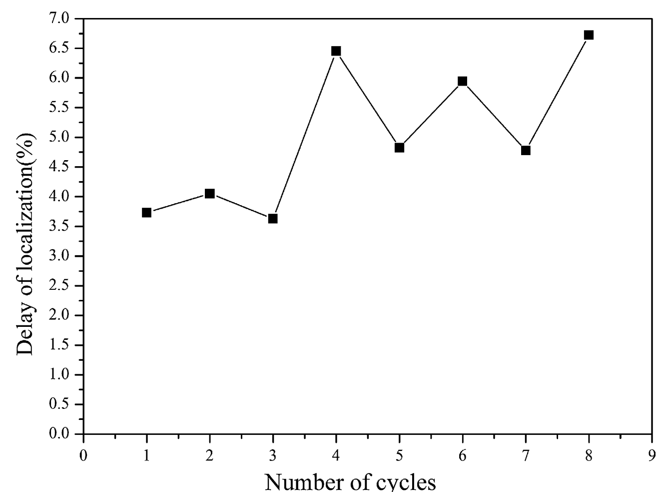

Fig. 8. Variations in localization delay with the number of ARB cycles in Ag100 group.

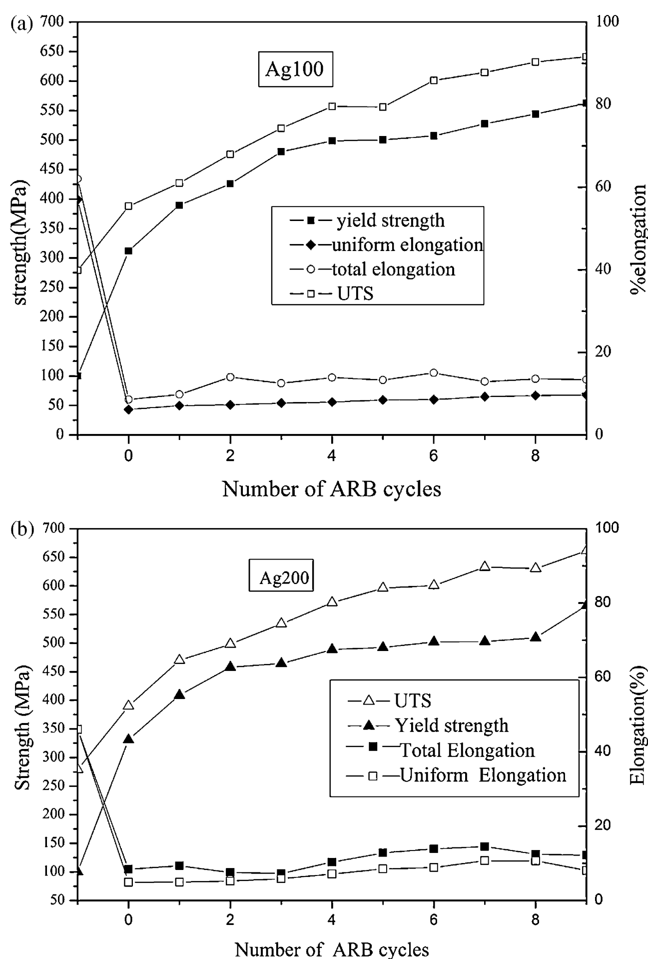

Fig. 9. Tensile properties of the ARB-processed: (a) Ag100 and (b) Ag200 sheets as a function of the number of ARB cycles.

strength of the 9-ARB cycle of Ag200 and Ag100 specimens was 661 and 641 MPa, respectively. This was 2.7 and 2.3 times higher than that of the primary copper sheet, respectively. As can be seen, due to the higher thickness of silver layers, the strength of the Ag200 group is higher than that of the Ag100 groups.

The flow stress of the roll-bonded material is composed of different strength contributions, notably strengthening owing to the deformation of microstructure and the presence of a multilayer structure.

i. Strengthening due to the deformation of microstructure

Deformation of microstructure plays an important role in strengthening via several mechanisms at different strain levels:

a. Strengthening due to large deformation

Two strengthening mechanisms can contribute to the strengthening during the large deformation of materials. The first one is the strengthening caused by the presence of incidental dislocation boundaries (IDBs) with a small misorientation ($\leq 3^{\circ}$). These boundaries arise from the statistical trapping of dislocations. The second mechanism is the grain boundary strengthening via the Hall–Petch relationship by the formation of geometrically necessary boundaries (GNBs) arising from the difference in the slip system operating in the neighboring slip systems or the local strain difference within each grain [32].

b. Strengthening due to strain hardening

At the early stage of the ARB process, strain hardening plays an important role in strengthening. As mentioned before, by increasing the ARB cycles, strain hardening is decreased and the gradual formation of the ultrafine grained structure plays the main role in strengthening.

c. Strengthening due to shear strain

There are two other possible mechanisms in the ARB process, which differ from other high straining processes. The first possible mechanism is the effect of a severe shear deformation just below the surface. It has been reported that the severe shear deformation is introduced by the friction between the work piece and the roll under dry conditions. This shear deformation significantly increases the equivalent strain and promotes grain refinement. Moreover, the ARB process can introduce this severely deformed region into the interior of the material by repetition. The whole thickness of materials may be severely strained after several cycles. The other mechanism is the introduction of new interfaces. A large number of interfaces are introduced by several ARB cycles. These interfaces show a well-developed fiber structure [20].

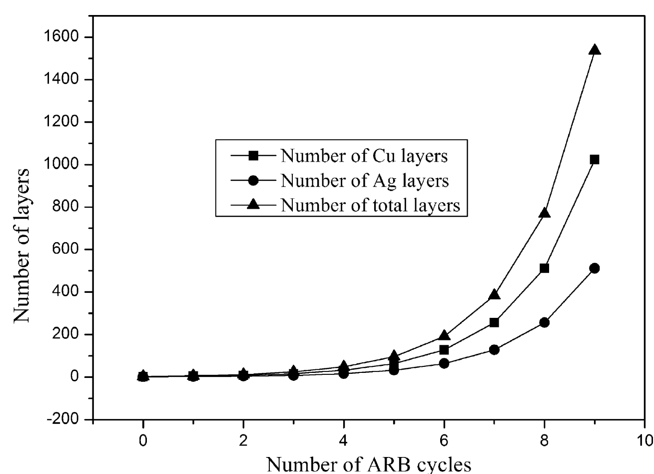

Fig. 10. Variation in the number of ARB layers by increasing the ARB cycles.

ii. Strengthening due to the presence of a multilayer structure

In the present research a Cu–Ag multilayer was produced by the ARB process.

This multilayer structure has an important role in the strengthening of the samples via two mechanisms:

a. Residual stresses

In this method residual stresses are introduced between layers as a result of the co-deformation of Cu–Ag sheets subjected to a large plastic strain. These stresses may directly influence the multilayer strength by affecting the dislocation motion. Although the Ag layer has the same face-centered-cubic (fcc) crystallographic structure as Cu, it has a smaller elastic modulus and a larger lattice parameter than Cu. Therefore, the incompatibility between the two phases may influence the co-deformation mode of the component in the composites. The meticulous explanation of the co-deformation of the ARB-processed Cu–Ag sheets is a subject to be studied in future.

b. The number of layers and their thicknesses

As a result of increasing the number of ARB cycles, the thickness of the layers decreases and the number of layers per unit thickness increases. This layer refinement affects the strength of the produced multilayer via the so-called Hall–Petch relationship. Figs. 10 and 11 show variations in the number of layers and thicknesses vs. the ARB cycles, respectively. As can be seen, at the initial stages of process the variation in the layer thickness is high, while at the final stages of ARB the number of layers increases exponentially. Therefore, at the

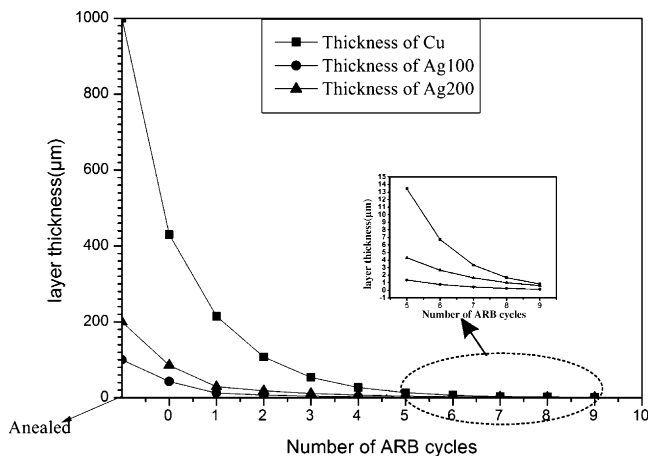

Fig. 11. Variation in the thickness of the ARB layers by increasing the ARB cycles.

former stages, the layer thickness and at the latter stages, the number of layers contributes to strengthening.

3.3. Electrical resistivity

Fig. 12 shows the electrical resistivity variations of the two groups of the ARB-processed sheets measured in various cycles. As can be seen, the electrical resistivity of both groups is almost close to that of the pure copper in the first cycles. Note that the electrical resistivity was measured from the surface of the samples. The outer layer of all samples was copper and the thickness of the copper layer in the first cycles was rather high. Therefore, most of the conducting electrons pass through copper and the effect of silver is negligible. In the final cycles, where the copper layers become very thin, it seems that the silver layers pronounce some effect and the electrical resistivity differs from that of Ag100 and a slight increase in resistivity of Ag100 is observed. The observed fluctuations in the early cycles can be due to measurement errors or layers delamination.

The variation in the strain level hence the dislocation density and the number of Cu–Ag interfaces during the ARB process can change the electrical resistivity.

The effect of dislocation density on electrical resistivity results from the scattering of the electrons by the dislocations core. The applied DC four-point-probe technique is not sensitive enough to take into account the effect of dislocations core [33]. Therefore the main contribution to the electrical resistivity change is the interface scattering of the conducting electrons. As a result, the electrical resistivity of Ag100 samples is increased slightly by increasing the number of cycles. The electrical resistivity of Ag200 is lower than that of Ag100, because the silver layers are thicker and higher in content in Ag200 group.

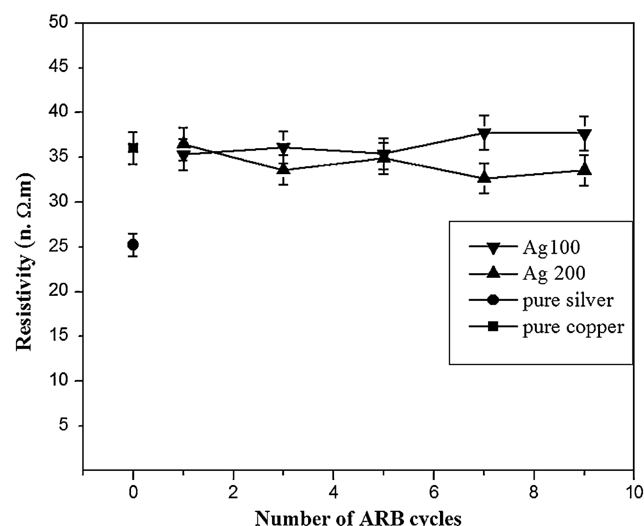

Fig. 12. Variation of electrical conductivity of produced Cu/Ag nanocomposites by various ARB cycles.

4. Conclusions

The ARB process is a suitable method for producing the Cu/Ag nanocomposite multilayers. By combining the two most conductive metals, Ag and Cu, a composite with extremely high electrical conductivity and high-strength was produced by this method for the first time. The strength of the produced nanocomposites was higher than that of the primary copper and silver sheets. The continuity of the constituent layers was maintained up to the ninth cycle owing to the low hardness and high thickness ratio of the two constituent phases. The slight increase in electrical resistivity of Ag100 was caused by electron scattering by interfaces. The Ag200 samples had higher strength and higher electrical conductivity than the Ag100 samples. Therefore, for high-strength and high-conductive applications it is reasonable to use the former. UFG microstructures were observed in the Cu–Ag samples after five ARB cycles.

References

[1] J. Lyubimova, J. Freudenbergera, C. Mickela, T. Thersleff, Mater. Sci. Eng. A 527 (2010) 606–613.
[2] L. Zhang, L. Meng, Scripta Mater. 52 (2005) 1187–1191.
[3] D.W. Yao, L. Meng, Physica B 403 (2008) 3384–3388.
[4] Z.C. Dettmer, M. Simmons, IEEE Trans. Magn. 39 (2003) 323–326.
[5] F. Misják, P.B. Barna, A.L. Tóth, T. Ujvári, I. Bertóti, G. Radnóczi, Thin Solid Films 516 (2008) 3931–3934.
[6] J.M. Zhang, G.X. Chen, K. Wei Xu, J. Alloys Compd. 425 (2006) 169–175.
[7] Y. Sakai, K. Inoue, T. Asano, H. Maeda, IEEE Trans. Magn. 28 (1992) 888–891.
[8] S. Nestorovic, I. Markovic, D. Markovic, Mater. Des. 31 (2010) 1644–1649.
[9] L. Meng, S.P. Zhou, F.T. Yang, D.Z. Lin, Mater. Res. Bull. 36 (2001) 1729–1735.
[10] S. Menzel, S. Strehle, H. Wendrock, K. Wetzig, Appl. Surf. Sci. 252 (2005) 211–214.
[11] J. McKeown, A. Misra, H. Kung, R.G. Hoagland, M. Nastasi, Scripta Mater. 46 (2002) 593–598.
[12] T. Spassov, L. Lyubenova, Y. Liu, S. Bliznakov, M. Spassova, N. Dimitrov, J. Alloys Compd. 478 (2009) 232–236.
[13] J.M. Zhang, G.X. Chen, K.W. Xu, J. Alloys Compd. 425 (2006) 169–175.
[14] S. Zghal, M.J. Hy¨tch, J.P. Chevalier, R. Twesten, F. Wu, P. Bellon, Acta Mater. 50 (2002) 4695–4709.
[15] S. Zghal, R. Twesten, F. Wu, P. Bellon, Acta Metall. 50 (2002) 4711–4726.
[16] T. Asano, Y. Sakai, M. Oshikiri, K. Tnoue, H. Maeda, IEEE Trans. Magn. 30 (1994) 2106–2109.
[17] Y.Z. Tian, X.H. An, S.D. Wu, Z.F. Zhang, R.B. Figueiredo, Scripta Mater. 63 (2010) 65–68.
[18] Y.G. Koa, S. Namgungb, B.U. Leeb, D.H. Shinb, J. Alloys Compd. (2010), doi:10.1016/j.jallcom.2010.02.050.
[19] M. Eizadjou, H. Danesh Manesh, K. Janghorban, J. Alloys Compd. 474 (2009) 406–415.
[20] Y. Saito, H. Utsunomiya, N. Tsuji, T. Saka, Acta Mater. 47 (1999) 579–583.
[21] A. Mozaffari, H. Danesh Manesh, K. Janghorban, J. Alloys Compd. 489 (2010) 103–109.
[22] Y.F. Sun, N. Tsuji, H. Fujii, F.S. Li, J. Alloys Compd. (2010), doi:10.1016/j.jallcom.2010.02.201.
[23] M. Alizadeh, M.H. Paydar, J. Alloys Compd. 492 (2010) 231–235.
[24] M. Eizadju, A. Kazemi Talachi, H. Danesh Manesh, H. Shakur Shahabi, K. Janghrban, Compos. Sci. Technol. 68 (2008) 2003–2009.
[25] S. Ohsaki, S. Kato, N. Tsuji, T. Ohkubo, K. Hono, Acta Mater. 55 (2007) 2885–2895.
[26] G.K. Williamson, W.H. Hall, Acta Metall. 1 (1953) 22–31.
[27] D. Yang, J. Xiong, P. Hodgson, Mater. Lett. 63 (2009) 2300–2302.
[28] J.M. Lee, B.R. Lee, S.B. Kang, Mater. Sci. Eng. A 406 (2005) 95–101.
[29] A. Mashreghi, L. Ghalandari, M. Reihanian, M.M. Moshksar, Mater. Sci. Forum 633–634 (2010) 131–150.
[30] H.W. Kim, S.B. Kang, N. Tsuji, Y. Minamino, Acta Mater. 53 (2005) 1737–1749.
[31] D.R. Metzger, X. Duan, M. Jain, D.S. Wilkinson, R. Mishra, S. Kim, A.K. Sachdev, Mech. Mater. 38 (2006) 1026–1038.
[32] M. Reihanian, R. Ebrahimi, N. Tsuji, M.M. Moshksar, Mater. Sci. Eng. A 473 (2008) 189–194.
[33] D. Mattissen, D. Raabe, F. Heringhaus, Acta Mater. 47 (1999) 1627–1634.